Available online at www.sciencedirect.com
SCIENCE DIRECT®
Physics of the Earth and Planetary Interiors 143–144 (2004) 481–495
PHYSICS OF THE EARTH AND PLANETARY INTERIORS
www.elsevier.com/locate/pepi

The structure of amorphous iron at high pressures to 67 GPa measured in a diamond anvil cell

Guoyin Shen [a,*], Mark L. Rivers [a], Stephen R. Sutton [a], Nagayoshi Sata [a], Vitali B. Prakapenka [a], James Oxley [b], Kenneth S. Suslick [b]

[a] *Consortium for Advanced Radiation Sources, University of Chicago, Chicago, IL 60637, USA*
[b] *School of Chemical Sciences, University of Illinois at Urbana-Champaign, Urbana, IL 61801, USA*

Received 18 December 2002; received in revised form 24 April 2003; accepted 2 May 2003

Abstract

We report the results of room temperature compression studies of amorphous iron up to 67 GPa. The experiments were performed with a modified diamond anvil cell (DAC) that allows for measurements of X-ray scattering to a maximum momentum of 86.6 nm^{-1} using a monochromatic beam at a wavelength of 0.3311 Å. It is shown that accurate structural determination can be made for amorphous materials in a DAC to ultra high pressures. The dense random-packing model is favored to interpret our observations for amorphous iron. The resultant structure factor and the pair distribution function show that the dominant peak does not significantly change in shape and in intensity with the increase of pressure, except for peak positions. This observation is consistent with essentially zero pressure dependence of the coordination number and ratios of distances derived from the obtained pair distribution functions at high pressures. It is thus proposed that the structural contraction with the increase of pressure for amorphous iron is isotropic, which allows us to estimate volume changes as a function of pressure from the positions of the first peak in the pair distribution function. The compression behavior is found to be similar to those of b.c.c.-Fe and h.c.p.-Fe.

Keywords: Amorphous structure; Iron; High pressure; Diamond anvil cell

1. Introduction

Iron is believed to be the major constituent of the Earth's core (Birch, 1964) of which more than 96% by volume is in a liquid state. It is therefore of great geophysical interest to study the behavior of liquid iron at high pressures and high temperatures. Extensive investigations have been made by shock-wave (Ahrens and Johnson, 1995; Brown et al., 2000), static compression (Sanloup et al., 2000) and theoretical simulations (Alfe et al., 2000, 2002; Anderson and Ahrens, 1994). Information on the liquid structure provides a basis for investigating numerous macroscopic physical properties such as viscosity and self-diffusion (atomic transport) (Alfe et al., 2000; Brazhkin and Lyapin, 2000; Zhang and Guo, 2000; Zhang et al., 2000), electrical resistivity (electron transport) (Ashcroft and Lekner, 1965; March, 1990), compressibility (Ascarelli, 1968; Hasegawa and Watabe, 1972; Trigger et al., 1994) and thermal expansion (Hasegawa and Watabe, 1974). Such properties of the outer core are key parameters needed for modeling

* Corresponding author. Tel.: +1-630-252-0429; fax: +1-630-252-0436.
E-mail address: shen@cars.uchicago.edu (G. Shen).

0031-9201/$ – see front matter © 2004 Elsevier B.V. All rights reserved.
doi:10.1016/j.pepi.2003.05.004

the dynamo, geomagnetism, composition and thermal state.

The structure of liquid iron has been extensively studied by theory (Alfe et al., 2000, 2002; Hausleitner and Hafner, 1989; Stixrude and Brown, 1998). Direct experimental study of the structure of liquid iron is limited to ambient pressure (Waseda and Suzuki, 1970) and to a pressure of 5 GPa with a large volume press (Sanloup et al., 2000) by X-ray scattering. Two major difficulties exist in liquid scattering experiments at high pressures. One is technical, arising from the extreme pressure–temperature (*P–T*) conditions required. The other difficulty with liquid scattering is the large background signal generated by the pressure vessel. Recently major progress has been made in the generation and control of extreme *P–T* conditions both in large volume presses (Kubo et al., 2004) and in the diamond anvil cell (DAC) (Dubrovinsky et al., 2000; Mao and Hemley, 1996; Shen et al., 2001). It is now possible to extend the measurements to extreme conditions approaching those of the outer core. To overcome the second difficulty of large background, spatial collimation is generally introduced to reduce the scattering from the pressure vessel. For example, with the energy dispersive technique, X-ray scattering is measured at a fixed angle (Katayama et al., 2000; Kruger and Meade, 1997; Meade et al., 1992; Tsuji et al., 1989). This method involves data collection at several 2θ angles and intensity normalization to the X-ray source spectrum. Recently Eggert et al. (2002) used monochromatic X-ray beam and reported structure factors of liquids (argon and water) in a DAC. Multichannel collimators have been developed with large volume presses (Mezouar et al., 2002; Yaoita et al., 1997), which allows structural studies of non-crystalline materials with the angle dispersive technique. The use of a monochromatic beam greatly increases the quality of structure factor determination for amorphous materials. In this paper, we present the structure determinations of amorphous iron with a monochromatic X-ray beam.

The structure of amorphous metals (metallic glasses) is very close to that of liquid metals (Waseda, 1980). There is a strong geophysical motivation to study the behavior of amorphous iron at high pressure. In contrast to the extensive experimental high pressure studies of crystalline iron (Boehler, 1993; Brown et al., 2000; Dubrovinsky et al., 2000; Hemley and Mao, 2001; Jephcoat et al., 1986; Mao et al., 1990; Shen et al., 1998), no high pressure work has been reported for amorphous iron, presumably because of the lack of availability of samples and difficulties involved in X-ray scattering measurements. Amorphous iron of high purity has been successfully synthesized sonochemically (Suslick et al., 1991). Neutron scattering has been used to study the structure of the amorphous iron at ambient pressure (Bellissent et al., 1993). The structure of thin films of amorphous iron have been investigated using transmission electron diffraction (Ichikawa, 1973; Leung and Wright, 1974). In this article we report the results of a room temperature compression study on amorphous iron up to 67 GPa using a monochromatic synchrotron beam and a modified DAC suitable for studies of amorphous materials at very high pressures. Accurate structure determinations are presented and the effect of pressure on the structure is shown.

2. Experiment

The amorphous iron sample was prepared sonochemically (Suslick et al., 1991). Bulk elemental analysis determined the iron powder to be >96 wt.% iron with a trace amount of carbon (<3 wt.%) and oxygen (<1 wt.%). The sample can be easily oxidized. Therefore, the sample loading was performed in a glove box filled with inert gas (argon), which provides an atmosphere of <1 ppm O_2.

A boron nitride seat (purchased from Linatec, Ukraine) was employed for high X-ray transmission over the full aperture of the DAC. The DAC used in this study is a symmetrical cell (Mao et al., 1998) with a full access opening angle of 60°. In the case of loading axis parallel to the incident X-ray beam in the present study, the maximum 2θ is 30°. With a monochromatic beam at a wavelength of 0.3311 Å, the maximum momentum transfer ($Q_{max} = 4\pi \sin\theta_{max}/\lambda$) is $\sim$98 nm^{-1}. In the present study, the value of Q_{max} is found to be 86.6 nm^{-1}.

The sample configuration is shown in Fig. 1. Type-IA diamond was used for the anvils, with a culet size of 300 μm in diameter. A stainless steel gasket with initial thickness of 250 μm was used, and pre-indented to a thickness of $\sim$30 μm. A hole of 300 μm in diameter was drilled and then filled

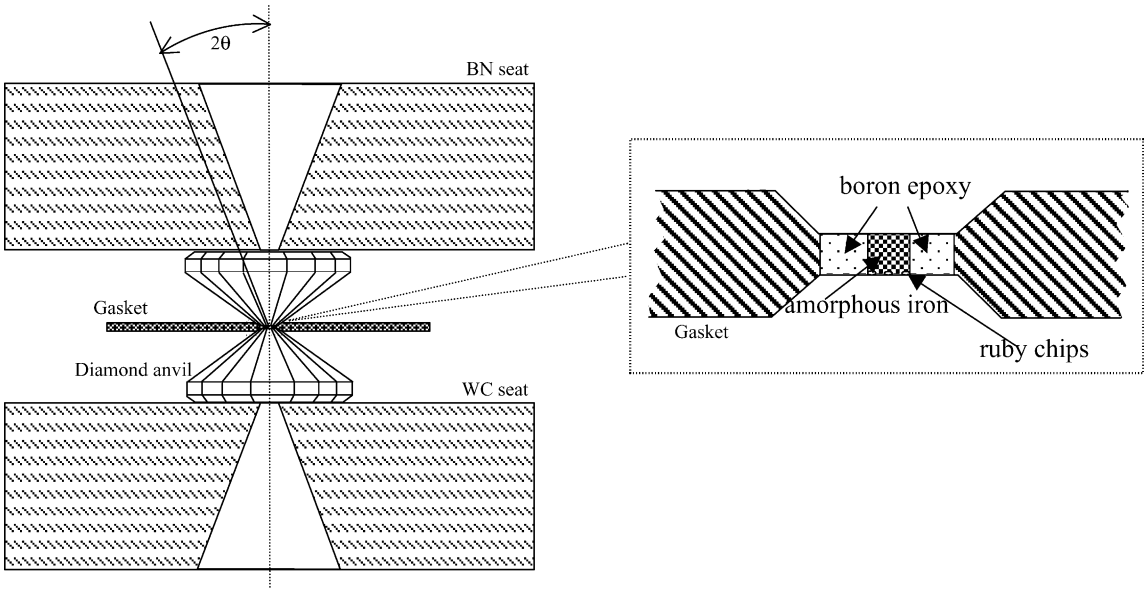

Fig. 1. Schematic of the diamond anvil cell used in this study. One seat is made of boron nitride for a large X-ray access opening. Enlarged figure shows the amorphous-boron insert gasket configuration, which helps in increasing the sample thickness and in performing proper background subtraction.

with amorphous-boron epoxy (epoxy to boron ratio of 1:2 by weight). The filled boron epoxy was then compressed by diamond anvils to a few GPa, and a 100 μm hole was drilled in the pressed boron epoxy. Finally the amorphous sample was loaded in the hole. A few ruby chips were also loaded for pressure measurement. The whole assemblage was sealed in a glove box by increasing pressures to a few GPa. The boron insert gasket helps to collect weak X-ray scattering from amorphous materials free of contamination from gasket diffraction. It also helps to make reliable background subtraction using the empty cell, without worries about gasket hole deformation.

X-ray diffraction experiments were performed at 13 BM-D at the advanced photon source. We used a 1 m long focusing mirror in the vertical direction and 0.1 m long mirror in the horizontal direction to focus the beam at the sample position to a size of 10 μm (horizontal) × 27 (vertical) μm at full width half maximum. A Bruker 2K-CCD detector was used to collect X-ray scattering. Typical exposure time was 10 min. Multiple exposures (2–3 times) were made for better statistics at high pressures. The sample-detector distance and the detector tilt angles were calibrated using powder diffraction from a CeO_2 standard that was placed at the sample position with the help of a microscope. The 2D images were angularly integrated by using the program FIT2D (Hammersley et al., 1996), and all geometric and polarization corrections were made during the integration. In cases where a few diffraction spots arose from the ruby chips, masks were used in the integration.

After reaching to a maximum pressure of 67 GPa, pressure was released and the sample was removed from the gasket hole. The same gasket was then put back in the cell, and the empty cell reference was measured with geometry identical to that at high pressures with help of a kinematic base.

3. Data analysis

3.1. Data reduction to atomic units

The description of the atomic distribution in non-crystalline materials usually employs the concepts of the structure factor and the pair distribution function in atomic units. The measured X-ray scattering intensity is in arbitrary units and needs to be converted into atomic units to describe the structure.

The observed X-ray scattering intensity is the combination of sample and background contributions:

$$I^{\mathrm{obs}}(Q) = a(Q)I^{\mathrm{samp}}(Q) + bI^{\mathrm{back}}(Q) \quad (1)$$

where $Q = 4\pi \sin(\theta)/\lambda$ is the scattering momentum, $a(Q)$ the diamond anvil cell transmission, b the scale factor for background correction, $I^{\mathrm{samp}}(Q)$ the scattering from the sample, and $I^{\mathrm{back}}(Q)$ the background scattering from the same DAC without sample. The transmission $a(Q)$ can be calculated according to the cell dimensions and absorption coefficients of materials involved. The factor b is determined as follows (Fig. 2). At values of Q larger than 86.6 nm^{-1}, the sample signal is blocked by the cell body. The intensity in this region should be zero, a criterion used for determining the factor b. The subtracted pattern is also checked for reasonableness in the small-Q region. When an oscillation was observed in the small-Q region due to slight mislocation of the beam stop, a linear fit was applied to remove the oscillation. Eq. (1) allows us to obtain the scattering from the sample: $I^{\mathrm{samp}}(Q)$.

By introducing a normalization factor N, the total scattering from the sample $I^{\mathrm{samp}}(Q)$ can be expressed in atomic units by the coherent scattering $I^{\mathrm{coh}}(Q)$, incoherent scattering $I^{\mathrm{incoh}}(Q)$, and the multiple scattering $I^{\mathrm{mul}}(Q)$ (Waseda, 1980):

$$NI^{\mathrm{samp}}(Q) = I^{\mathrm{coh}}(Q) + I^{\mathrm{incoh}}(Q) + I^{\mathrm{mul}}(Q) \quad (2)$$

The incoherent scattering contribution can be computed using the analytic formulas (Balyuzi, 1975; Thakkar and Chapman, 1975). The multiple scattering is generally neglected in X-ray diffraction (Waseda, 1980). By definition, the structure factor is obtained from the coherent scattering: $S(Q) \equiv I^{\mathrm{coh}}(Q)/f^2(Q)$,

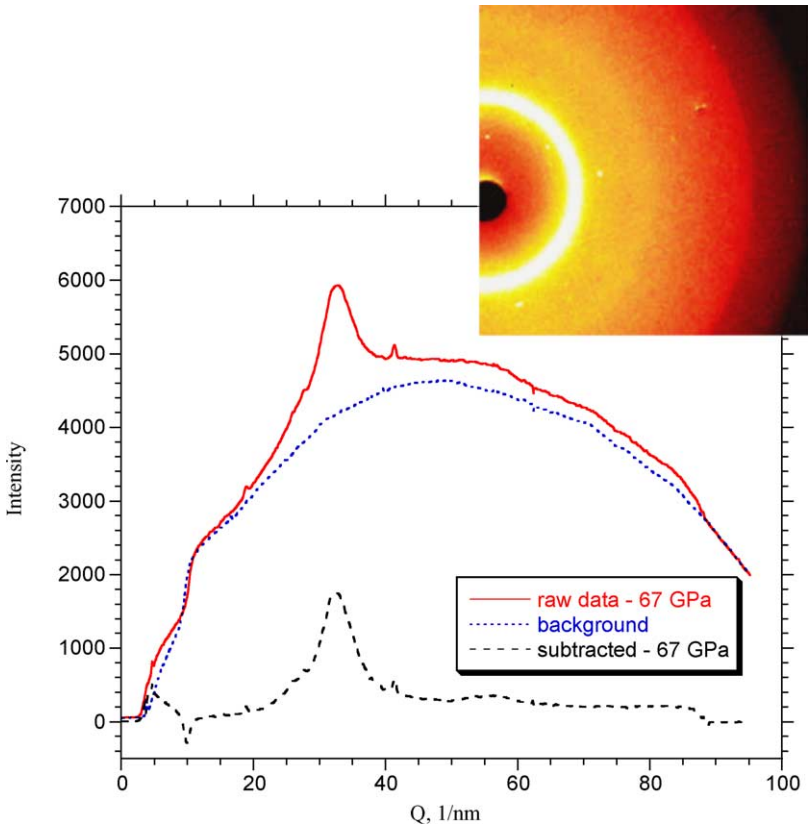

Fig. 2. Illustration of the background subtraction. An integrated pattern of X-ray scattering for amorphous iron at 67 GPa is plotted together with the empty cell background and the background subtracted pattern, with the factor b in Eq. (1) being 0.715. The insert is the background subtracted image at 67 GPa.

where $f(Q)$ is the atomic scattering factor (International Tables of Crystallography).

We determine the normalization factor N by using Krogh–Moe–Norman method (Krogh-Moe, 1956; Norman, 1957)

$$N = \frac{\int_0^{Q_{\max}} Q^2 \left\{ [f^2(Q) + I^{\text{incoh}}(Q)] \frac{\exp(-\gamma Q^2)}{f^2(Q)} \right\} \times \mathrm{d}Q - 2\pi^2 n_0}{\int_0^{Q_{\max}} Q^2 \left[I^{\text{samp}}(Q) \frac{\exp(-\gamma Q^2)}{f^2(Q)} \right] \mathrm{d}Q} \tag{3}$$

where n_0 is the average atomic number density of the sample. The damping factor $\exp(-\gamma Q^2)$ is introduced to reduce errors in the high-Q region due to the factor Q^2 in Eq. (3) (Waseda, 1980). γ of 0.001 was used in the present study. By definition, the structure factor is then calculated by

$$S(Q) = \frac{1}{f^2(Q)} \left\{ N \left[\frac{I^{\text{obs}}(Q) - bI^{\text{back}}(Q)}{a(Q)} \right] - I^{\text{incoh}}(Q) \right\} \tag{4}$$

The Fourier transformation of $Q[S(Q) - 1]$ is the distribution function in real space:

$$F(r) \equiv 4\pi r n(r) - 4\pi r n_0 = \frac{2}{\pi} \int_0^{Q_{\max}} Q[S(Q) - 1] \sin(rQ)\, \mathrm{d}Q \tag{5}$$

where $n(r)$ is the function of atomic number density. From $F(r)$, the pair distribution function $g(r)$ is obtained:

$$g(r) = 1 + \frac{F(r)}{4\pi n_0 r} \tag{6}$$

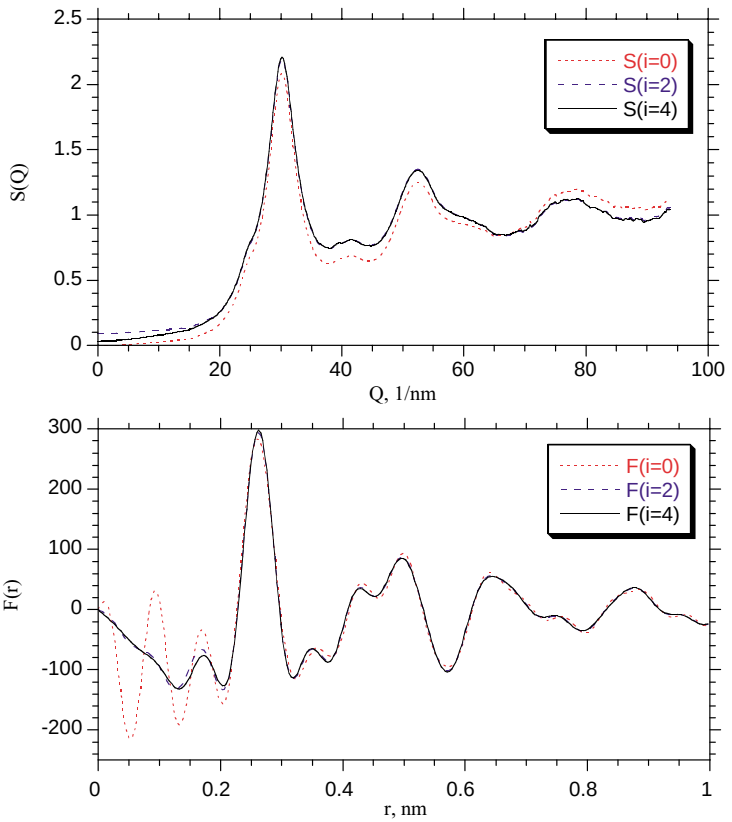

Fig. 3. Iteration evolutions of the structure factor $S_{(i)}(Q)$ and the distribution function $F_{(i)}(r)$ for amorphous iron at ambient pressure. $F_{(0)}(r)$ shows oscillations in the small-r region due to errors in $S(Q)$. Note that these oscillations quickly converge after a few iterations.

3.2. Optimization procedure

Since the atoms do not approach each other within the atomic core diameter, $n(r)$ should be zero in this region. Therefore, from Eq. (5) we have

$$F(r) = -4\pi r n_0 \quad (\text{small } r) \tag{7}$$

From this Kaplow et al. (1965) and Eggert et al. (2002) proposed a refinement procedure for $S(Q)$ and $g(r)$. The refinement procedure is based on the observation that errors in $F(r)$ due to uncertainties in $S(Q)$ are dominant in the small-r region. The relation (Eq. (7)) can be used as an iterative feedback to determine a corrected value for $S(Q)$. Following their approaches, we established an iterative procedure for analyzing the amorphous iron data. According to Eqs. (5) and (7), we have

$$F_{(i)}(r) = \frac{2}{\pi}\int_0^{Q_{\max}} Q[S_{(i)}(Q) - 1]\sin(rQ)\,\mathrm{d}Q \tag{8}$$

$$\Delta F_{(i)}(r) = F_{(i)}(r) + 4\pi r n_0 \quad (r < r_{\min}) \tag{9}$$

where $r_{\min}$ is a value close to the atomic radius, i denotes iteration number. An improved $S_{(i+1)}(Q)$ can then be obtained by applying the Fourier transformation of $\Delta F_{(i)}(r)$:

$$S_{(i+1)}(Q) = S_{(i)}(Q) - \frac{1}{Q}\int_0^{r_{\min}} \Delta F_{(i)}(r)\sin(rQ)\,\mathrm{d}r \tag{10}$$

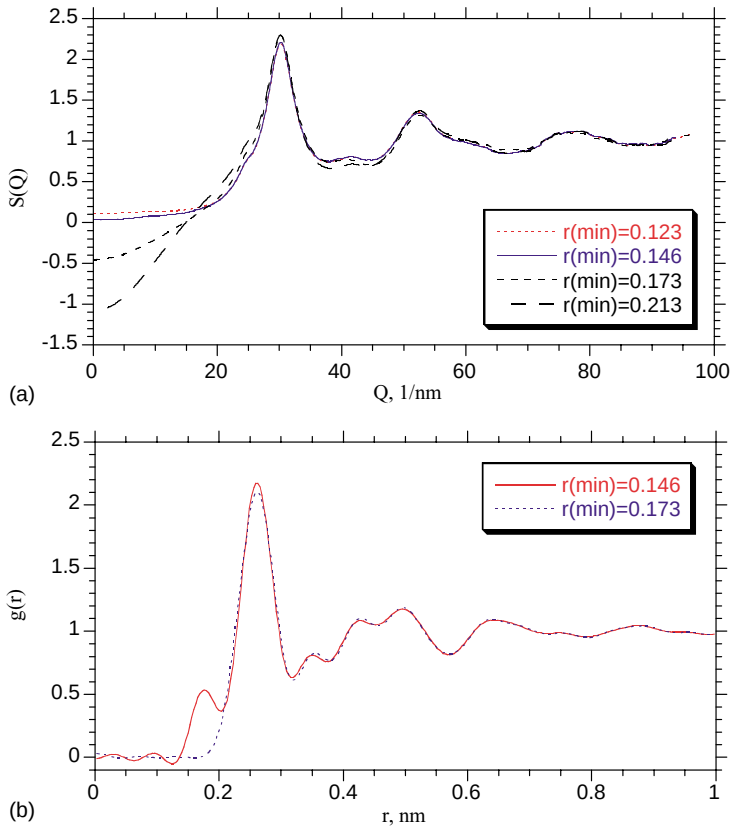

Fig. 4. Behavior of the optimized structure factor $S(Q)$ and the pair distribution function $g(r)$ as a function of $r_{\min}$ (Eqs. (9) and (10)) for amorphous iron at ambient pressure. The small peak below the dominant peak in $g(r)$ may be removed by using values of $r_{\min}$ larger than 0.176 nm. However, the resultant $S(Q)$ becomes unphysical. Reasonable $S(Q)$ is obtained with $r_{\min}$ of 0.146 nm, a number close to atomic core radius. Numbers in the figure are in units of nm.

This process is found to be effective and convergence is rapid as shown in Fig. 3.

The above process requires the value of atomic density n_0. In this study, n_0 at high pressures are from a separate work using the X-ray absorption method. This method has been successfully used for determinations of densities of liquids in a DAC (Shen et al., 2002a). Eggert et al. (2002) estimated n_0 by minimizing a chi-squared misfit: $\chi^2 \equiv \int_0^{r_{\min}} [\Delta F_{(i)}(r)]^2 \, dr$, for high pressure fluids (argon and water), where i is the iteration number. This could be significant because it provides a method for measuring equations of state for amorphous materials from determinations of the structure factor. However, we found that the values of χ^2 is extremely sensitive to $r_{\min}$ in Eq. (10). The determined n_0 in this way could be unphysical without strong constraints on $r_{\min}$.

3.3. Effects of $r_{\min}$ and $Q_{\max}$

While spurious oscillations in the distribution function $F(r)$ at small values of r can be effectively removed by applying the above optimization procedure (Fig. 3), it is necessary to perform reliability checks for the corrected $S(Q)$. We make use of two criteria: (1) in the small-Q region, $\lim_{Q\to 0} S(Q) = S(0) = n_0 k_B T\beta$, where k_B is the Boltzmann constant, β the isothermal compressibility and T the absolute temperature; (2) the corrected $S(Q)$ must be compared with the original data within experimental errors.

For example, as shown in Fig. 4, a peak at around 0.16 nm below the first peak in $g(r)$ can be removed by having $r_{\min}$ larger than 0.176 nm. However, the resultant $S(Q)$ with $r_{\min}$ larger than 0.176 nm becomes negative at small-Q, in conflict with the criterion (1) mentioned above. The optimum $S(Q)$ is then found at

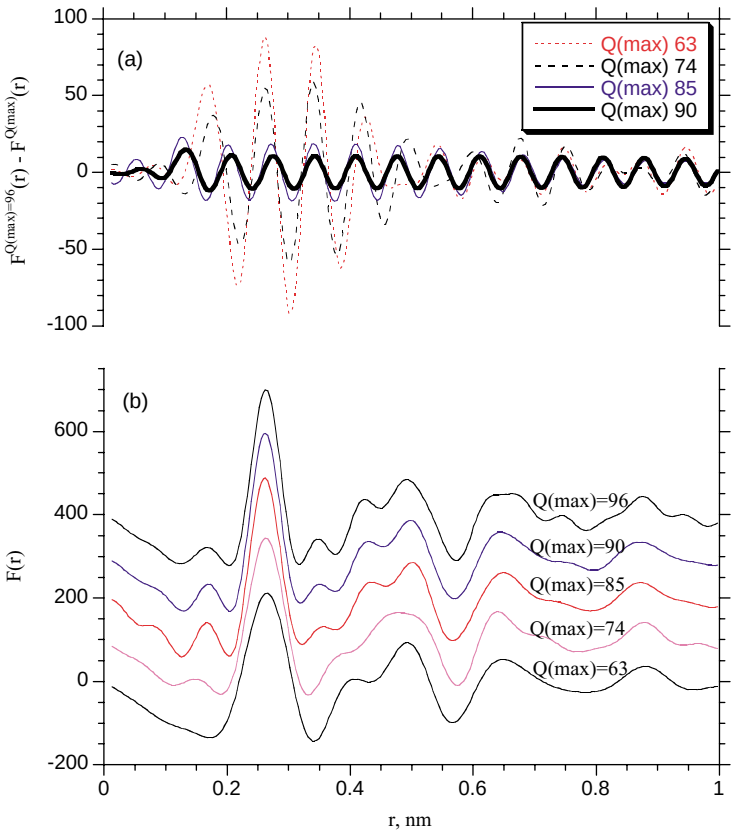

Fig. 5. Truncation effect of $Q_{\max}$ on the distribution function $F(r)$. The differences in $F(r)$ are shown in (a). Note that the large oscillations are in the vicinity of the first dominant peak. Numbers in the figure are in units of nm^{-1}.

r_{min} 0.146 nm, a number close to atomic core radius, leaving a small peak in $g(r)$ at around 0.16 nm which might arise from the truncation effect in Fourier transformation as discussed below.

The truncation of the experimental data at Q_{max} is a limiting factor to derive accurate information in real space. This is especially true for high pressure studies because of the limited scattering angle accessible with high pressure instruments. The truncation could lead to ghost peaks in $F(r)$, and their positions are functions of Q_{max}. For example, based on Waseda (1980), the ghost maxima are at distances about $\pm(5/4)(2\pi/Q_{max}), \pm(9/4)(2\pi/Q_{max}), \ldots$ from the main peak position. As shown in Fig. 5b, the distribution functions in real space are plotted from the data with different values of Q_{max}. With increasing values of Q_{max}, two sub-peaks beside the dominant peak shift close to the main peak, and their positions are close to the ghost maxima. Thus, these two sub-peaks are interpreted as not real but ghost peaks from the truncation effect. At values of Q_{max} larger than 85 nm^{-1}, we found that the general pattern remains the same, with a slight increase in peak resolution as value of Q_{max} increases. Practically speaking, it is helpful to terminate $S(Q)$ at several values of Q less than the experimental limit of Q_{max} and to check the resultant effects on $F(r)$. However, it is still difficult to state the accuracy of the obtained distribution functions. Large Q-range coverage will clearly help on this matter.

The differences in $F(r)$ with various Q_{max} values, the relative to that with Q_{max} of 96 nm^{-1}, are plotted in Fig. 5a. The resultant error results in oscillations with an approximate period of $2\pi/Q_{max}$. It is noted that the greatest oscillation occurs in the vicinity of the first peak, where it holds the most critical information (Fig. 5a). Again it shows that large Q coverage is important in experiments. In the present study, Q_{max} value of 96 nm^{-1} is used for the data at ambient pressure and Q_{max} value of 86.6 nm^{-1} for data at high pressures.

4. Results and discussions

4.1. Data at ambient pressure

The prepared sample is very sensitive to oxygen, to a level of only a few ppm (Suslick et al., 1991). For high pressure measurements, the sample was well sealed by two diamond anvils and free from oxygen contamination. Interestingly, in our experiments after compression to a maximum pressure of 67 GPa, the sample was removed from the DAC in air and the X-ray scattering pattern was found to be consistent with those for the sample in the cell and also with the neutron scattering data (Bellissent et al., 1993). This indicates that the recovered sample is still amorphous iron, providing X-ray scattering data at ambient pressure. The oxidation resistance could be due to high compression under ultra high pressures for this initially porous sample. After compression in the DAC, the compact sample has two surfaces as shiny as diamond anvils, which may retard the sample oxidation. This is the first time that such sample has been preserved in air, and it is achieved with high pressure compression.

The recorded data were analyzed with the procedures mentioned above. Since the data were collected with the sample outside the DAC, $a(Q)$ and b in Eq. (1) are both unity. The sample's self-absorption effect is neglected in this study because the sample thickness is only on the order of 10 μm. Change in absorption over Q-range to 100 nm^{-1} is less than 0.1% for an iron sample with a thickness of 10 μm at 37.44 keV. Fig. 6 shows the structure factor and the pair distribution function of the amorphous iron at ambient pressure, together with the data of liquid iron at 1833 K (Waseda and Suzuki, 1970) for comparison.

4.2. High pressure data

The structure factor and the pair distribution function at high pressures are summarized in Fig. 7. Q_{max} of 86.6 nm^{-1} is used to derive $g(r)$ for all pressures, including that at ambient pressure. It is found that with increasing pressure the peak height of $S(Q)$ (Fig. 7a) remains essentially the same, although the peak position shifts to a higher Q value. Similar features were found in $g(r)$ in real space. The peak height in $g(r)$ does not significantly change with increase of pressure, while the peak position shifts to a smaller r values, an indication of compression. Peak positions in $g(r)$ are summarized in Table 1.

With the concept of the nearest coordination number (CN), we may describe the picture of the nearest neighbor atoms in a quantitative way. There is no

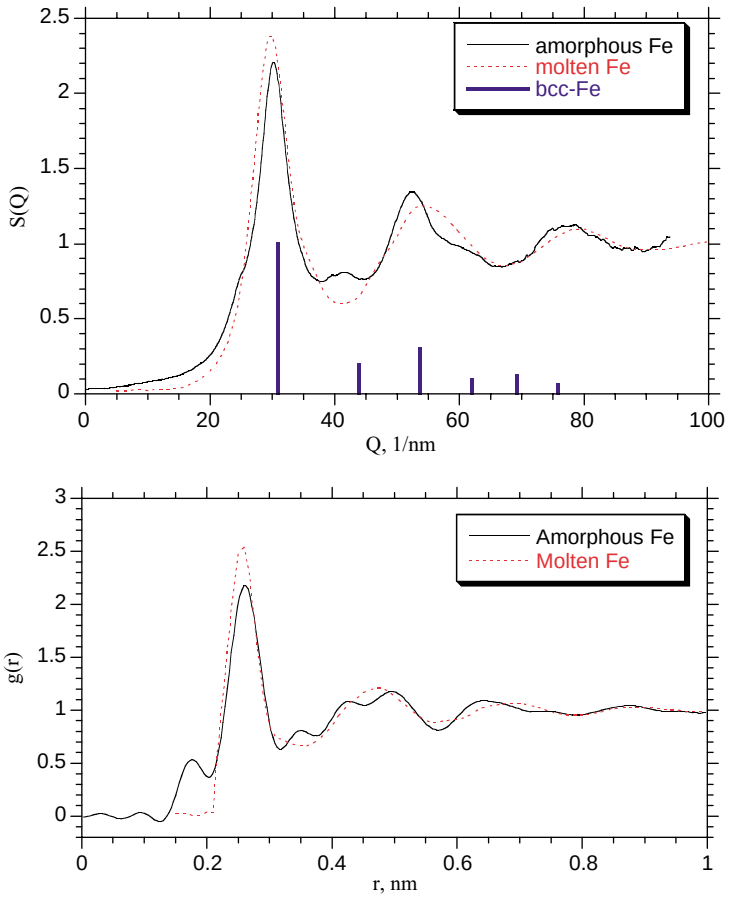

Fig. 6. The structure factor $S(Q)$ and the pair distribution function $g(r)$ of amorphous iron at ambient pressure. Data for liquid iron (Waseda and Suzuki, 1970) and crystalline b.c.c.-Fe are shown for comparison.

unique method of estimating the coordination number. In this study, it is assumed that the coordination shell is symmetric about a radius that defines the maximum in the $4\pi r^2 g(r)$ curve, the so-called radial distribution function. Thus the coordination number is determined from the integration:

$$\mathrm{CN} = 2n_0 \int_{r_0}^{r_{\max}} 4\pi r^2 g(r)\,\mathrm{d}r \qquad (11)$$

where r_0 is the left-hand edge of the first peak and $r_{\max}$ the peak value of r in the $4\pi r^2 g(r)$ curve. The calculated coordination numbers as a function of pressure are plotted in Fig. 8. No clear coordination number change is found with increase of pressure within experimental uncertainties, a result consistent with the observation that the peak height and the peak width in $g(r)$ do not change significantly with pressure.

4.3. The structure of amorphous iron

As shown in Fig. 6, the general structural feature of the amorphous state is similar to that of the liquid state except for a few weak peaks. In the liquid state, the amplitude of the atomic vibration is large, leading to a large uncertainty in the position of the lattice point, thus resulting in an averaged smooth distribution in both $S(Q)$ and $g(r)$ (Fig. 6). On the other hand, the small amplitude of vibration of atoms in the amorphous state contributes to the construction of a more fixed atomic arrangement, causing some small peaks in $S(Q)$ and $g(r)$ (Fig. 6).

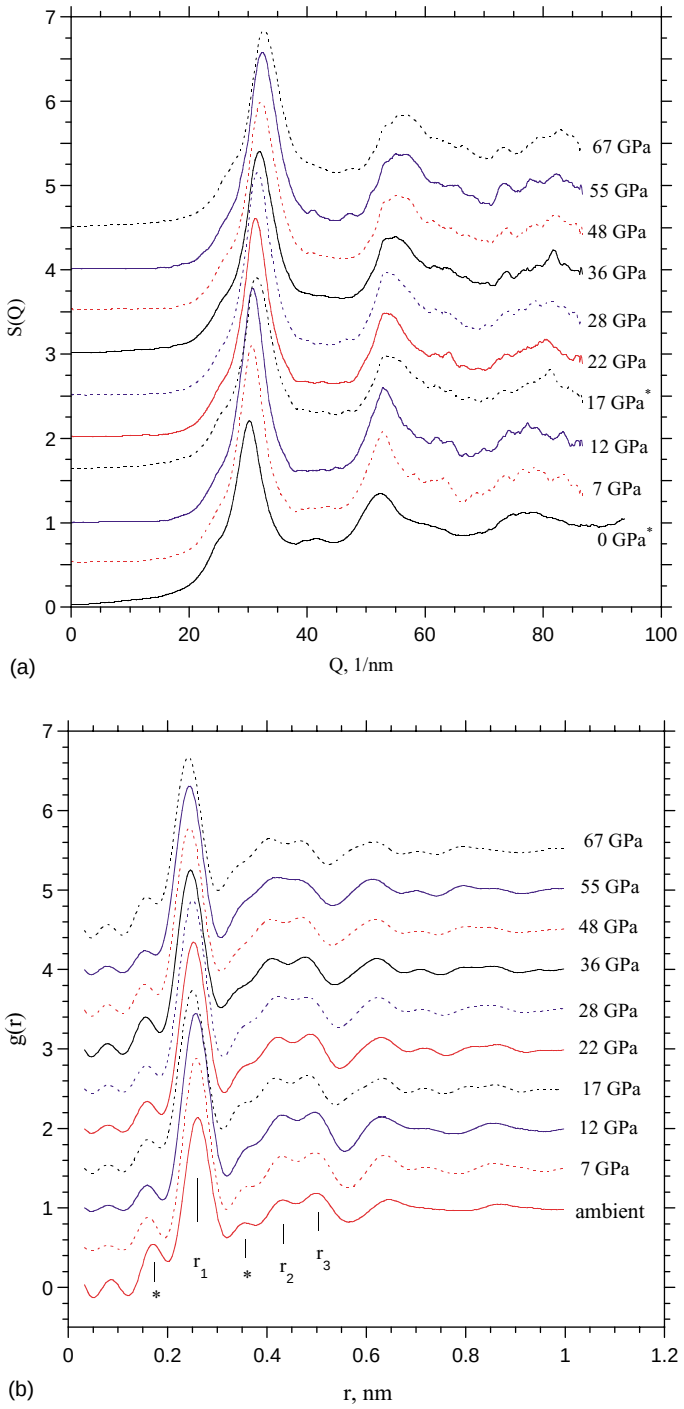

Fig. 7. (a) The structure factor $S(Q)$ at high pressures. (b) The pair distribution function $g(r)$ at high pressures. An offset of 0.5 in both $S(Q)$ and $g(r)$ is applied between pressures for clarity. Peaks marked with (∗) may arise from the truncation effect (see text). No clear change in shape or intensity is observed for the dominant first peak in $S(Q)$ and $g(r)$, while the peak positions vary with pressure.

Table 1
Peak positions and calculated ratios of distances in $g(r)$ at various pressures

P (GPa)	CN atoms	r_1 (nm)	r_2 (nm)	r_3 (nm)	r_2/r_1	r_3/r_1
0[a]	9.3(4)	0.2644(13)	0.428(3)	0.500(4)	1.63	1.89
		0.256[b]	0.434[b]	0.496[b]	1.69[b]	1.93[b]
	10.6[c]	0.258[c]	0.48[c]		1.67[d,e]	1.96[d,e]
7	10.1(5)	0.2615(15)	0.430(3)	0.500(4)	1.64	1.91
12	11.0(5)	0.2616(15)	0.429(5)	0.499(5)	1.64	1.91
17[a]	9.9(5)	0.2547(15)	0.417(3)	0.485(3)	1.64	1.90
22	10.6(5)	0.2570(15)	0.421(3)	0.489(3)	1.64	1.90
28	10.9(5)	0.2549(15)	0.419(3)	0.483(3)	1.64	1.89
36	10.0(5)	0.2507(15)	0.408(3)	0.480(3)	1.63	1.91
48	10.5(5)	0.2489(15)	0.404(3)	0.474(3)	1.62	1.90
55	11.1(5)	0.2492(15)	0.414(5)	0.476(4)	1.66	1.91
67	10.5(5)	0.2462(15)	0.404(3)	0.469(3)	1.64	1.90

[a] Data collected on decreasing pressure.
[b] Bellissent et al. (1993).
[c] Waseda and Suzuki (1970).
[d] Leung and Wright (1974).
[e] Ichikawa (1973).

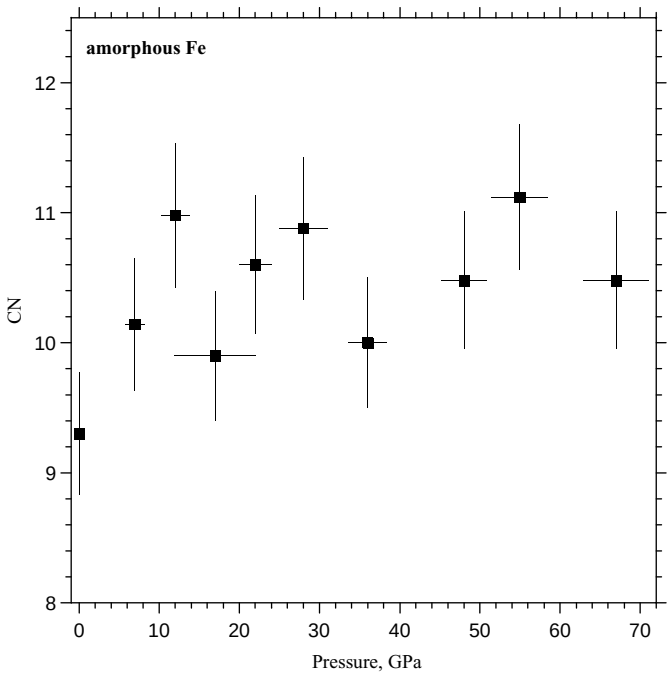

Fig. 8. The nearest neighbor coordination (CN) number as a function of pressure, determined according to Eq. (11). No pressure dependence is observed within experimental uncertainties, with an average number at 10.5(5). Errors in CN are estimated to be 5%. Errors in pressures are from multiple ruby fluorescence measurements in the region of 30 μm around the sample.

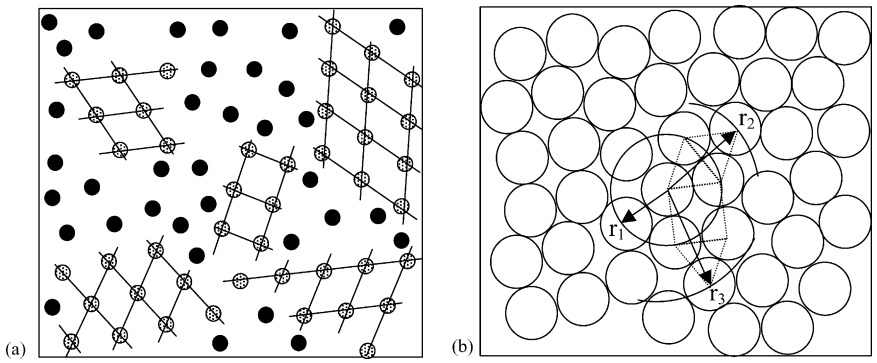

Fig. 9. Models for the amorphous structure: (a) a structure consisting of microcrystalline fragments randomly orientated and distributed; (b) a dense random-packing (DRP) model. The DRP model is favored from this study. r_1, r_2, and r_3 shown in the figure are assigned to peaks in $g(r)$ shown in Fig. 7b.

There are two models in the literature for amorphous structures, the microcrystalline disorder model and the topological disorder model (Waseda, 1980) (Fig. 9). Studies on thin films of amorphous iron showed that the later type describes the amorphous structure well (Ichikawa, 1973; Leung and Wright, 1974). Ichikawa (1973) suggested a dense random-packing model (DRP), in which the structure is built by packing of essentially irregular assemblages of basic polyhedra, such as tetrahedra and octahedra, without vacancy and long-range order. From this study, our data also support the concept of a truly amorphous phase devoid of crystalline order based on the following findings. (1) No noticeable change in shape is observed in $S(Q)$ or $g(r)$ with increase of pressure (Fig. 7). The ratios of the distances in Table 1 are essentially constant as a function of pressure. These observations disfavor the microcrystalline disorder model because crystalline iron undergoes a phase transition at around 12 GPa (b.c.c. to h.c.p. phase transition), and the phase change would affect the pattern shape and the radial distances in $g(r)$ according to the calculations of Ichikawa (1973). (2) As it can be seen in Table 1, the ratios of the distances between our data at ambient pressure and those from thin films result are in good agreement, suggesting an analogous structure.

The dominant peak (denoted as the r_1 peak) is found at around 0.25 nm (Figs. 6 and 7b). This peak can clearly be attributed to the nearest neighbors. The calculated coordination numbers (Fig. 8) of about 10.5(5) indicate that the amorphous state is densely packed.

According to the DRP model, the structure is constructed by serially and densely piling up regular or slightly distorted polyhedra (tetrahedra and octahedra) around a seed cluster (Ichikawa, 1973). The ratios of the distances of r_2/r_1 and r_3/r_1 for the amorphous iron in this study are found to be in the vicinity of 1.64 and 1.91, respectively (Table 1). The ratio of r_2/r_1 is very close to the c/a ratio in closed packed hexagonal structure ($c/a = 1.63$). The peak of r_2 is thus assigned to the basic tetrahedral unit. The close comparison to the ideal value indicates that the tetrahedra are regular by average. As shown in Fig. 9b, by combining octahedra and tetrahedra, the distance r_3 is $\sim 1.90 r_1$. This combination produces a ratio close to the measured value of r_3/r_1. Therefore, the basic polyhedra observed consist of tetrahedra and octahedra. The broad peaks in $g(r)$, always observed in amorphous materials, suggest that most of these polyhedra are slightly deformed.

4.4. High pressure compression

One feature of our high pressure data is that the dominant peak, both in $S(Q)$ and $g(r)$, does not significantly change with increase of pressure, except that the peak position shifts to a higher Q value and to a smaller r value, respectively. This observation is further confirmed by the derived coordination number and ratios of distances (Fig. 8, Table 1). Essentially no pressure dependence is observed for these numbers within experimental uncertainty. This implies that the contraction of the amorphous iron is isotropic under

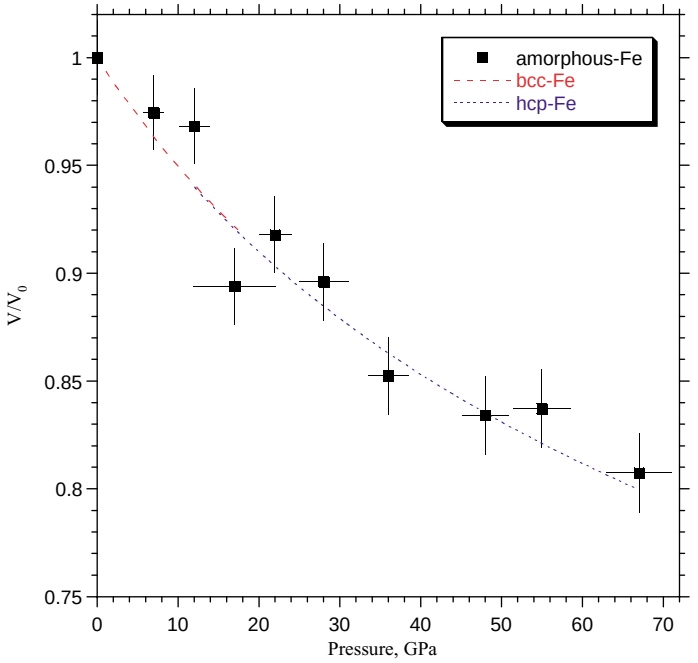

Fig. 10. High pressure volume compression of amorphous iron measured by the peak shift of the first peak in $g(r)$ (Fig. 7b). The validity of using the peak shifts to represent the volume changes is based on constant packing density as a function of pressure (Eq. (12)). The overall compression is comparable to the behaviors of b.c.c.-Fe and h.c.p.-Fe (Jephcoat et al., 1986; Mao et al., 1990).

pressure. By adopting the concept of the packing density (Ashcroft and Lekner, 1965)

$$\eta \equiv n_0 \frac{4}{3}\pi \left(\frac{1}{2}\sigma\right)^3 = \frac{1}{6} n_0 \pi \sigma^3 \quad (12)$$

where σ is the hard-sphere diameter, isotropic contraction means a constant packing density η with pressure. Indeed, by applying the hard-sphere model, coupled with the Percus–Yevick equation (Ashcroft and Lekner, 1965), to fit the first peak in $S(Q)$, we obtained η of 0.43(1) for all pressures up to 67 GPa.

From Eq. (12), isotropic contraction makes it possible to estimate densities of amorphous iron at high pressures according to the peak positions of r_1. Although the absolute values of r_1 might be different from the hard-sphere diameter σ in Eq. (12), the change of r_1 with pressure represents the decrease of σ. Fig. 10 shows the plot of $V/V_0[= r_1^3/(r_1^3)_{\text{ambient}}]$ as a function of pressure compared with the compression behaviors of b.c.c.-Fe (Jephcoat et al., 1986) and h.c.p.-Fe (Mao et al., 1990). Error bars in volume are from uncertainties in the peak fitting with a Gaussian function. Pressure error bars are from the gradients within 30 μm around the sample center. The overall compression is comparable to the behaviors of b.c.c.-Fe and h.c.p.-Fe. The data appear to be too scattered to fit with an equation of state. The scattering of data could be due to the stress effect arising from the pressure gradient, because no pressure medium was used in the present study to avoid unwanted scattering from other materials. The broad peak in $g(r)$ also limits the precision in determining the peak position.

It should be noted that the coordination number has been found to increase with pressure for many materials (Brown and Barnett, 1972; Shen et al., 2002b; Urakawa et al., 1999), especially for those with open structures (Funamori and Tsuji, 2002). In that case, caution should be taken in using Eq. (12) for estimating densities at high pressures (Brown and Barnett, 1972).

5. Conclusions

We have measured the structure of an amorphous iron sample of high purity at room temperature and at

pressures up to 67 GPa. A modified diamond anvil cell is used, allowing measurements of the X-ray scattering to a maximum momentum Q_{max} of 86.6 nm^{-1} with a monochromatic beam at a wavelength of 0.3311 Å. It is demonstrated that the weak scattering from the amorphous sample can be measured with the DAC up to ultra high pressures. By following the approaches of Eggert et al. (2002) and Kaplow et al. (1965), an optimization procedure is used to obtain accurate structural data of amorphous materials at high pressures. It is shown that spurious oscillations in $g(r)$ at the small-r region can be effectively corrected by applying this optimization procedure. It is also noted that truncation of the experimental data at Q_{max} is a limiting factor. Large Q coverage in experiments is desirable. Insufficient Q-range can cause inaccurate data in the pair distribution function $g(r)$, especially in the critical region around the first peak (Fig. 5).

The structure of amorphous iron is similar to that of liquid iron. A few peaks in $g(r)$ for the amorphous state are attributed to the construction of a more fixed atomic arrangement than in liquid. It is found that the dense random-packing model (Ichikawa, 1973) is favored to interpret our observations. From both the structure factor $S(Q)$ and the pair distribution function $g(r)$, the dominant peak does not significantly change in shape or intensity with increase of pressure, except that the peak position shifts to a higher Q value and to a smaller r value, respectively. This observation is consistent with the essentially zero pressure dependence of the coordination number (Fig. 8) and ratios of distances listed in Table 1, resulting in a conclusion of structurally isotropic contraction with pressure for amorphous iron. The isotropic contraction allows us to estimate the volume changes as a function of pressure from the positions of the first peak in the pair distribution function $g(r)$. The compression behavior at room temperature is found to be similar to those of b.c.c.-Fe and h.c.p.-Fe (Jephcoat et al., 1986; Mao et al., 1990) (Fig. 10).

Acknowledgements

Thanks are due to Jennifer Jackson, Jason Nicholas, and Stas Sinogeikin for the help during sample loading, Peter Eng in X-ray scattering experiments. Comments by Jennifer Jackson, Satoru Urakawa, and Nobumasa Funamori improved the manuscript. This work is supported by NSF-EAR 0001149 and 0229987. The GSECARS sector is supported by the National Science Foundation (Earth Sciences Instrumentation and Facilities Program) and Department of Energy-Basic Energy Sciences (Geoscience Program).

References

Ahrens, T.J., Johnson, M.L., 1995. Shock wave data for minerals. In: Ahrens, T.J. (Ed.), A Handbook of Physical Constants: Mineral Physics and Crystallography. American Geophysical Union, Washington, DC, pp. 143–184.

Alfe, D., Kresse, G., Gillan, M.J., 2000. Structure and dynamics of liquid iron at the pressures of the Earth's core conditions. Phys. Rev. B 61, 132–142.

Alfe, D., Price, G.D., Gillan, M.J., 2002. Iron under Earth's core conditions: Liquid-state thermodynamics and high-pressure melting curve from ab initio calculations. Phys. Rev. B 65, 165118.

Anderson, W.W., Ahrens, T.J., 1994. An equation of state for liquid iron and implications for the Earth's core. Rev. Geophys. 99, 4273–4284.

Ascarelli, P., 1968. Velocity of sound and compressibility in liquid metals. Phys. Rev. 173, 271–274.

Ashcroft, N.W., Lekner, J., 1965. Structure and resistivity of liquid metals. Phys. Rev. 145, 83–90.

Balyuzi, H.H.M., 1975. Analytic approximations to incoherent scattered X-ray intensities. Acta Cryst. A 31, 600–602.

Bellissent, R., Galli, G., Grinstaff, M.W., Migliardo, P., Suslick, K.S., 1993. Neutron diffraction on amorphous iron powder. Phys. Rev. B 48, 15797–15800.

Birch, F., 1964. Density and composition of the mantle and core. J. Geophys. Res. 69, 4377–4388.

Boehler, R., 1993. Temperatures in the Earth's core from melting-point measurements of iron at high static pressures. Nature 363, 534–536.

Brazhkin, V.V., Lyapin, A.G., 2000. Universal viscosity growth in metallic melts at megabar pressures: the vitreous state of the Earth's inner core. Phys. Uspekhi 43, 493–508.

Brown, J.M., Fritz, J.N., Hixson, R.S., 2000. Hugoniot data for iron. J. Appl. Phys. 88, 5496–5498.

Brown, K.H., Barnett, J.D., 1972. X-ray diffraction studies on liquids at very high pressures along the melting curve. II. Sodium. J. Chem. Phys. 57, 2016–2021.

Dubrovinsky, L.S., Saxena, S.K., Tutti, F., Rekhi, S., Lebehan, T., 2000. In situ X-ray study of thermal expansion and phase transition of iron at multimegabar pressure. Phys. Rev. Lett. 84, 1720–1723.

Eggert, J.H., Weck, G., Loubeyre, P., Mezouar, M., 2002. Quantitative structure factor and density measurements of high-pressure fluids in diamond anvil cells by X-ray diffraction: argon and water. Phys. Rev. B 65, 174105.

Funamori, N., Tsuji, K., 2002. Pressure-induced structural change of liquid silicon. Phys. Rev. Lett. 88, 255508.

Hammersley, A.P., Sevsson, S.O., Hanfland, M., Fitch, A.N., Häusermann, D., 1996. Two-dimensional detector software: from real detector to idealised image or two-theta scan. High Pressure Res. 14, 235–248.

Hasegawa, M., Watabe, M., 1972. Theory of compressibility of simple liquid metals. J. Phys. Soc. Jpn. 32, 14–28.

Hasegawa, M., Watabe, M., 1974. Theory of thermodynamic properties of liquid metals. J. Phys. Soc. Jpn. 36, 1510–1515.

Hausleitner, C., Hafner, J., 1989. A theoretical study of the melting curve of iron to very high pressure. J. Phys.: Condensed Matter 1, 5243–5352.

Hemley, R.J., Mao, H.K., 2001. In situ studies of iron under pressure: new windows on the Earth's core. Int. Geol. Rev. 43, 1–30.

Ichikawa, T., 1973. Electron diffraction study of the local atomic arrangement in amorphous iron and nickel films. Phys. Stat. Solidi A 19, 707–716.

Jephcoat, A.P., Mao, H.K., Bell, P.M., 1986. Static compression of iron to 78 GPa with rare gas solids as pressure-transmitting media. J. Geophys. Res. 91, 4677–4684.

Kaplow, R., Strong, S.L., Averbach, B.L., 1965. Radial density functions for liquid mercury and lead. Phys. Rev. 138, A1336–A1345.

Katayama, Y., et al., 2000. A first order liquid–liquid phase transition in phosphorus. Nature 403, 170–173.

Krogh-Moe, J., 1956. A method for converting experimental X-ray intensities to an absolute scale. Acta Cryst. 9, 951–953.

Kruger, M.B., Meade, C., 1997. High-pressure structural study of GeI_4. Phys. Rev. B 55, 1–3.

Kubo, A., et al., 2003. Phase equilibrium study of iron using sintered diamond (SD) anvils: absence of beta phase. PEPI, this volume.

Leung, P.K., Wright, J.G., 1974. Structural investigations of amorphous transition element films. II. Chromium, iron, manganese and nickel. Phil. Mag. 30, 995–1008.

Mao, H.K., Hemley, R.J., 1996. Experimental studies of Earth's deep interior: accuracy and versatility of diamond-anvil cells. Phil. Trans. Roy. Soc. Lond. A 354, 1315–1332.

Mao, H.K., Shen, G., Hemley, R.J., Duffy, T.S., 1998. X-ray diffraction with a double hot plate laser heated diamond cell. In: Manghnani, M.H., Yagi, T. (Eds.), Properties of Earth and Planetary Materials. AGU, Washington, DC, pp. 27–34.

Mao, H.K., Wu, Y., Chen, L.C., Shu, J.F., Jephcoat, A.P., 1990. Static compression of iron to 300 GPa and $Fe_{0.8}Ni_{0.2}$ alloy to 260 GPa: implications for composition of the core. J. Geophys. Res. 95, 21737–21742.

March, N.H., 1990. Liquid Metals: Concepts and Theory. Cambridge University Press, Cambridge, 492 pp.

Meade, C., Hemley, R.J., Mao, H.K., 1992. High pressure X-ray diffraction of SiO_2 glass. Phys. Rev. Lett. 69, 1387–1390.

Mezouar, M., et al., 2002. Multichannel collimator for structural investigation of liquids and amorphous materials at high pressures and temperatures. Rev. Sci. Instrum. 73, 3570–3574.

Norman, N., 1957. The Fourier transform method for normalizing intensities. Acta Cryst. 10, 370–373.

Sanloup, C., et al., 2000. Structural changes in liquid Fe at high pressures and high temperatures from synchrotron X-ray diffraction. Europhys. Lett. 52, 151–157.

Shen, G., Mao, H.K., Hemley, R.J., Duffy, T.S., Rivers, M.L., 1998. Melting and crystal structure of iron at high pressures. Geophys. Res. Lett. 25, 373–376.

Shen, G., Rivers, M.L., Wang, Y., Sutton, S.J., 2001. A laser heated diamond cell system at the advanced photon source for in situ X-ray measurements at high pressure and temperature. Rev. Sci. Instrum. 72, 1273–1282.

Shen, G., Sata, N., Newville, M., Rivers, M.L., Sutton, S.R., 2002a. Molar volumes of liquids measured in a diamond anvil cell. Appl. Phys. Lett. 81, 1411–1413.

Shen, G., et al., 2002b. Melting studies of indium: determination of structure and density of melts at high pressures and high temperatures. J. Phys.: Condensed Matter 14, 1–9.

Stixrude, L., Brown, J.M., 1998. The Earth's core. In: Hemley, R.J. (Ed.), Ultrahigh-pressure Mineralogy. Mineralogical Society of America, Washington, DC, pp. 261–282.

Suslick, K.S., Choet, S.B., Cichowlas, A.A., Grinstaff, M.W., 1991. Sonochemical synthesis of amorphous iron. Nature 353, 414–416.

Thakkar, J., Chapman, D.C., 1975. A new analytic approximation to atomic incoherent X-ray scattering intensities. Acta Cryst. A 31, 391–392.

Trigger, S.A., Bobrov, V.B., Vlasov, Y.P., 1994. Liquid metal compressibility theory using the OCP model as a reference system. Physica B 193, 291–294.

Tsuji, K., Yaoita, K., Imai, M., Shimomura, O., Kikegawa, T., 1989. Measurements of X-ray diffraction for liquid metals under high pressure. Rev. Sci. Instrum. 60, 2425–2428.

Urakawa, S., Igawa, N., Shimomura, O., Ohno, H., 1999. High pressure X-ray diffraction study on the structure of NaCl melt using synchrotron radiation. Am. Mineral. 84, 341–344.

Waseda, Y., 1980. The Structure of Non-crystalline Materials. McGraw-Hill, International Book Co, New York.

Waseda, Y., Suzuki, K., 1970. Atomic distribution and magnetic moment in liquid iron by neutron diffraction. Phys. Stat. Solidi 39, 669–678.

Yaoita, K., Katayama, Y., Tsuji, K., Kikegawa, T., Shimomura, O., 1997. Angle-dispersive diffraction measurement system for high-pressure experiments using a multichannel collimator. Rev. Sci. Instrum. 68, 2106–2110.

Zhang, Y.G., Guo, G.J., 2000. Molecular dynamics calculation of the bulk viscosity of liquid iron–nickel alloy and the mechanism for the bulk attenuation of seismic waves in the Earth's outer core. Phys. Earth Planet. Inter. 122, 289–298.

Zhang, Y.G., Guo, G.J., Nie, G.Z., 2000. A molecular dynamics study of the bulk and shear viscosity of liquid iron using embedded-atom potential. Phys. Chem. Mineral. 27, 164–169.